Materials Advances

ROYAL SOCIETY OF CHEMISTRY

PAPER

View Article Online
View Journal | View Issue

Cite this: *Mater. Adv.*, 2026, 7, 1250

Studies of release kinetics and antibacterial activity on pH-responsive core–shell microparticles loaded with lactoferrin

Teresa Paduano, †[ab] Michela Salamone, †[c] Federica Carraturo,[c] Simona Zuppolini, *[a] Mauro Zarrelli,[a] Aldobenedetto Zotti,[a] Rosa Vitiello,[b] Marika Avitabile,[b] C. Valeria L. Giosafatto,[b] Marco Guida,[c] Riccardo Tesser[b] and Anna Borriello[a]

Innovative delivery platforms based on biopolymer matrices are attracting increasing interest as effective tools to enhance the protection, solubility, and therapeutic outcome of sensitive bioactive compounds and macromolecules. This research focuses on the formulation and study of multilayered microsystems composed of naturally occurring polymers – specifically, alginate and chitosan – designed to encapsulate and gradually release lactoferrin, a multifunctional iron-binding glycoprotein with potent antimicrobial properties. Particularly, the iron-free lactoferrin form (apo-lactoferrin) plays a key role in the innate immune defense by exerting antimicrobial activity through two primary mechanisms: bacteriostatic and bactericidal. Lactoferrin-loaded microspheres were produced using a gentle ionic gelation technique and subsequently coated with a positively charged chitosan layer to maintain protein stability and regulate its release. Detailed morphological, thermal and physicochemical characterization studies were performed, along with release kinetics studies under various pH conditions. Additionally, the antimicrobial activity of the system was tested against clinically relevant bacterial strains, including *S. aureus*, *P. aeruginosa* and *E. coli*, at variable proton concentrations. The results showed that this core–shell platform enhances protein stability and selectively increases the antimicrobial efficacy under different pH conditions, demonstrating its potential for targeted intervention in infection-prone tissues with altered pH profiles. These findings suggest promising applications in pH-responsive topical treatments, particularly for managing chronic wounds and infection-prone tissues, where local pH alterations influence antimicrobial efficacy.

Received 6th August 2025,
Accepted 6th December 2025

DOI: 10.1039/d5ma00864f

rsc.li/materials-advances

1. Introduction

The use of polymer systems for the controlled release of bioactive agents represents a well-established strategy to enhance the stability, bioavailability, and pharmacological efficacy of labile compounds and proteins.[1] In particular, natural biopolymers have demonstrated significant advantages in the delivery of such macromolecular drugs, proven especially beneficial for therapeutic protein delivery, as they allow for the adjustment of the physicochemical properties of the carrier materials, thereby improving protein stability and therapeutic efficacy.[2] However, in recent years, scientific interest has increasingly shifted toward exploring the antimicrobial potential of these systems, focusing on the interactions between biomaterials and pathogenic microorganisms in response to the growing need for alternative therapeutic strategies to conventional antibiotics.[3] Among the most used biopolymers, sodium alginate stands out for its high biocompatibility, biodegradability, low cost, and pH sensitivity, making it an ideal candidate for encapsulating bioactive molecules through ionic gelation with divalent cations (*i.e.*, Ca^{2+}, Sr^{2+}, and Ba^{2+}).[4] The resulting particles protect proteins against adverse environmental conditions and regulate their release *via* diffusion across the polymeric matrix.[5] In a previous study, an alginate microparticle (ALG) system loaded with lactoferrin (Lf) was prepared using a one-phase ionic gelation procedure, and the release profile of the protein was examined in neutral and weakly acidic environments (pH = 5), highlighting rapid and poorly controlled release kinetics under acidic conditions.[6]

[a] *Institute for Polymers, Composites and Biomaterials (IPCB)-National Research Council, I-80055 Portici, Italy. E-mail: simona.zuppolini@cnr.it*
[b] *University of Naples Federico II, Department of Chemical Sciences, 80126, Naples, Italy*
[c] *University of Naples Federico II, Department of Biology, 80126, Naples, Italy*
† These authors contributed equally.

To address these limitations and achieve a more modulated and stable release, coating the microparticles with a second cationic polymer, such as chitosan, has been proposed.[7]

Chitosan (CHT) is a cationic polysaccharide that can interact with the carboxyl groups of alginate due to its protonatable amine groups,[8–10] forming core–shell structures with high mechanical stability, pH-sensitive behavior, and intrinsic antibacterial properties.[11] These characteristics make them especially suitable for delivering antimicrobial proteins in infected environments, where local pH can vary significantly.

In this work, core–shell microparticles based on alginate and chitosan—loaded with Lf—were designed, synthesized, and characterized through one-phase ionic gelation followed by cationic coating to enhance protein stability and optimize their release in response to pH variations.[12] The system underwent morphological, physicochemical, and kinetic characterization. Additionally, special attention was paid to evaluating the antibacterial activity of these microparticles and lactoferrin against *Staphylococcus aureus*, *Pseudomonas aeruginosa*, and *Escherichia coli* under various pH conditions.

Lf is a multifunctional glycoprotein with high iron-binding affinity, and is widely recognized for its potent antimicrobial properties. In this study, the focus was placed on the apo form of Lf (iron-depleted), which has demonstrated superior efficacy in inhibiting the growth and adhesion of both Gram-positive and Gram-negative bacteria, as well as in disrupting biofilm formation and intracellular invasion mechanisms.[13] Apo-Lf exhibits its antimicrobial activity through two distinct yet complementary mechanisms. The first is a bacteriostatic effect, achieved by chelating free iron from the surrounding environment, thereby depriving microorganisms of a critical element required for their metabolic processes.[14] The second mechanism is bactericidal and involves direct interaction with microbial membranes: the negatively charged apo-Lf molecule disrupts membrane integrity, leading to the leakage of intracellular contents and cell death. This dual functionality underscores its strong therapeutic potential, particularly in environments prone to infection. Given the increasing prevalence of antibiotic-resistant pathogens and the complexity of chronic wound environments, the development of smart delivery systems capable of pH-responsive release is of great clinical interest. Lf, with its natural antimicrobial and immunomodulatory properties, represents a valuable candidate for topical therapeutic strategies. In this context, we aimed to explore the potential of core–shell microstructures to enhance Lf stability and activity under variable pH conditions typically encountered in infected or damaged tissues. The objective was to investigate the effect of pH on the Lf release kinetics and the antimicrobial effectiveness of the particles, evaluating their potential application as advanced therapeutic agents. This work aimed to investigate the effect of pH on both the release kinetics of Lf and the antimicrobial effectiveness of the particles, evaluating their potential application as advanced therapeutic agents. The synergistic combination of the antimicrobial properties of Lf with the functional characteristics of the alginate-chitosan system represents a promising strategy for treating localized infections, particularly in biologically complex environments with variable pH.

2. Materials and methods

2.1. Materials

Sodium alginate (Manugel GHB, average MW 97 kDa, M/G ratio 0.59, FMC BioPolymers UK Ltd. Girvan, Ayrshire, KA269JN, UK), bovine iron-depleted (apo-)lactoferrin (total protein 95%, Fonterra, Auckland, New Zealand), chitosan (CHT, Medium MW, 75–85% deacetylation grade, Sigma Aldrich, Milan, Italy), acetic acid ($\geq$99.8%, ACS reagent) and anhydrous calcium chloride ($CaCl_2$) (Sigma Aldrich, Milan, Italy) were used as received for the preparation of microgels. Bi-distilled water, tris(hydroxymethyl)aminomethane hydrochloride (Tris-HCl) (Sigma Aldrich, Milan, Italy), and citric acid/sodium hydroxide (pH 5, VWR, Milan, Italy) buffer solutions were used for the release kinetics study.

2.2. Preparation of core–shell microparticles

Core–shell alginate–chitosan (ALG@CHT) microparticles were obtained by deposition of a CHT layer onto ALG microgel surfaces prepared according to the simple method reported in our previous work.[6] Briefly, 3 mL of sodium alginate solution (2 wt%) was added dropwise to 18 mL of $CaCl_2$ solution (0.1 M) under continuous stirring (200 rpm) at room temperature (25 $\pm$ 2 °C). After 15 min, the resulting crosslinked alginate microgels (ALG) were collected and washed three times with Millipore water. They were successively suspended in 30 mL of chitosan 0.5 wt% solution (previously prepared by dispersing chitosan in 1 wt% acetic acid) under continuous mild stirring (100 rpm) for 30 min. The neat ALG@CHT microgels obtained were collected and washed three times with Millipore water and freeze-dried. The collected washes were analyzed by UV-vis spectroscopy to define the encapsulation efficiency (EE%) and the loading capacity (LC) of Lf.

The same principle was followed to prepare Lf-loaded core–shell microgels (ALG:Lf@CHT). First, Lf-loaded alginate (ALG:Lf) microgels were prepared as reported, starting from a solution of both ALG and Lf components (previously prepared by mixing equal volumes of 2 wt% stock solutions in a 1 : 1 ratio) and stirring at 200 rpm for about 10 min until a uniform mixture was obtained.[6] The ALG:Lf microgels obtained were collected and washed with Millipore water and then suspended in 30 mL of chitosan solution under stirring (100 rpm) for 30 minutes. The resulting ALG:Lf@CHT microgels were collected, washed three times with Millipore water and freeze-dried.

2.3. Structural analysis

For structural analysis of the freeze-dried samples, attenuated total reflectance–Fourier transform infrared (ATR-FTIR) spectra were recorded on a Bruker Vertex V70 in the range of 4000–400 cm^{-1} with a resolution of 4 cm^{-1} and 32 scans.

2.4. Morphological analysis

The morphology of both swollen and freeze-dried samples (ALG@CHT and ALG:Lf@CHT) was first analyzed by optical

microscopy (using the Optical Olimpus BX51 Instrument) at different magnifications and then characterized by scanning electron microscopy (SEM) (FEI Quanta 200 FEG equipment, Hillsboro, OR, USA) under high vacuum conditions (20 kV). For SEM analysis all samples were previously metalized by depositing a 5/10 nm thick Au/Pd layer using an Emitech K575X sputter coater (Quorum Technologies Ltd, Kent, UK).

2.5. Thermal analysis

The thermal stability of the microparticles was evaluated by thermogravimetric analysis (TGA) using a Netzsch TG 29 F1 Libra system (Netzsch Geratebau GmbH, Selb, Germany) under a N2 atmosphere (50 mL min^{-1}). For this assay, approximately 6 mg (SD ± 0.5) of the samples were heated over a range from 25 °C to 800 °C with a heating ramp of 10 °C min^{-1}. Differential scanning calorimetry (DSC) analyses were carried out to assess the thermal behavior of the different formulations: ALG, ALG:Lf, ALG@CHT, and ALG:Lf@CHT. Approximately 5 ± 0.5 mg of each freeze-dried sample was accurately weighed and sealed in standard aluminum crucibles. The thermograms were recorded using a DSC Q1000 system by TA Instruments, under a nitrogen atmosphere (flow rate: 50 mL min^{-1}) to prevent oxidative degradation. The temperature program consisted of a first heating scan from −50 °C to 200 °C at a rate of 10 °C min^{-1}, followed by cooling from 200 °C to −50 °C with the same scanning rate, and finally a second heating from −50 °C to 300 °C.

2.6. Swelling index

The swelling index (Q%) of core–shell microparticles was measured *via* a gravimetric method. All the experiments were carried out in triplicate to determine the standard deviation (±SD). Weighed lyophilized microspheres were immersed in 3 mL of Millipore water at room temperature (25 ± 2 °C) and were weighed over time, after removal of the excess water with Whatman filter paper (Sigma Aldrich, Milan, Italy).[15] Q (%) of the microspheres was calculated using the following eqn (1):

$$Q\ (\%) = [(M_{sw} - M_d)/M_d] \times 100 \quad (1)$$

where M_{sw} is the weight of swollen microspheres at time t and M_d is the weight of dry microspheres, respectively.

2.7. Particle size measurement

The size distributions of the freshly prepared swollen microparticles (ALG@CHT and ALG:Lf@CHT) were determined using ImageJ 1.58 g software. The image analysis was based on the conversion of the pixel image value area in a user-defined section. The average size of the microspheres was reported as mean ± standard deviation (SD ±).

2.8. Microparticle diameter measurement and Z-potential analysis

The freeze-dried microparticles were analyzed by evaluating both the surface charge potential and particle size distribution using a Zetasizer Nano-ZSP (Malvern®, Worcestershire, UK) with a 633 nm wavelength and a 4 mW helium-neon laser, according to Avitabile *et al.* (2024).[16] The samples were diluted to 1 mg mL^{-1} in a citric acid/sodium hydroxide (pH 5.0) and Tris-HCl 10 mM (pH 8.5) buffer solution to assess their behavior under different pH conditions. The choice of these pH values was made to mimic physiological environments relevant for preventive medical applications, such as mild acidic conditions found in inflammatory sites or alkaline conditions present in certain biological fluids. It was not possible to evaluate the net charge of the particles at neutral pH since the particles at neutral pH were not soluble. The analysis was carried out at a temperature of (25 ± 2 °C), with an applied voltage of 200 mV. Zeta potential was determined by instrument software through the electrophoretic mobility at 200 mV, utilizing the Henry equation. The software also calculated the average particle diameter using dynamic light scattering (DLS) and the polydispersity index (PDI), which indicates the relative variation in particle size distribution. Zeta potential and particle size measurements were conducted in triplicate and all the results were reported as mean ± standard deviation (SD ±).

2.9. *In vitro* release tests

To investigate the Lf release profile and pattern, freeze-dried ALG:Lf@CHT microparticles were immersed in different pH solutions (pH 5, 7 and 8.5). A typical experiment was carried out by placing the freeze-dried sample in a buffer solution (with a definite volume of 40 mL). All the experiments were carried out at room temperature (25 ± 2 °C) under constant weak stirring (100 rpm) and were conducted in triplicate. At specific time intervals, an aliquot (3.0 mL of solution) from each sample was taken out to determine the concentration of released Lf using an Agilent Technologies Cary 60 UV-Vis spectrophotometer (Santa Clara, United States) at λ_{max} = 280 nm. The analyzed aliquot was added back to the stirring system to maintain a constant volume. The cumulative release of Lf (C%) *versus* time was plotted.

2.10. Encapsulation of lactoferrin (Lf)

To estimate the amount of Lf within the particles, the encapsulation efficiency (EE) and Loading capacity (LC) were determined using a UV-vis spectrophotometer at λ_{max} = 280 nm,[17] based on a previously established calibration curve (0.05–1 mg mL^{-1} concentration range). EE was calculated by the following eqn (2):

$$EE\ (\%) = [(m - mf)/m] \times 100 \quad (2)$$

where m is the initial total amount of Lf, and mf is the free amount of Lf calculated at zero time in the residual $CaCl_2$ crosslinking solution and washing fractions.

LC was calculated as the ratio between the mass of encapsulated Lf (mg) and the total mass of the dried particles (mg) in eqn (3):

$$LC\ (\%) = [(m - m_f)/m_p] \times 100 \quad (3)$$

where m is the initial total amount of Lf, m_f is the free amount of Lf, and m_p is the mass of the dried particles. All

measurements were performed in triplicate and are reported as mean values ± standard deviation (SD ±).

2.11. Antimicrobial activity assay

The antibacterial activity of apo-Lf, core–shell ALG@CHT, and ALG:Lf@CHT microparticles against *S. aureus* ATCC®, *P. aeruginosa* ATCC® 9027 and *E. coli* ATCC® 25922 was investigated. These bacteria are some of the pathogens that appear in the case of epithelial wounds and can significantly impede wound healing, negatively affecting the healing process.[18]

Three pH conditions (5, 7, and 8.5) were tested at different incubation times.

The Lf free and encapsulated concentrations were 0.5 mg mL^{-1}. Different incubation times were evaluated, depending on the *in vitro* release kinetics tests at various pH levels. Based on the specific growth requirements of each microorganism, individual cultures of the three bacterial strains were incubated under the following conditions: *S. aureus* ATCC® 6538 was grown for 24-48 h at 37 °C[19]; *P. aeruginosa* ATCC® 9027 was incubated for 24 h at 37 ± 1 °C;[20] and *E. coli* ATCC® 25922 was cultured for 24 h at 37 ± 1 °C.[21] All microbial suspensions were maintained under constant agitation at 200 rpm in 30 mL tryptic soy broth (TSB, Thermo Fisher Scientific, USA). To standardize the bacterial concentration to 10^8 cells per mL, the optical density was measured at 560 nm using a spectrophotometer (Hach Lange DR6000, Hach, USA), with an OD value of 1.125 corresponding to the desired cell density. The bacterial suspensions were then serially diluted to achieve a target concentration of 10^7 CFU per mL in 10 mL. The experimental procedure was designed following UNI EN 1276: 2020,[22] employing the time-kill assay described by Alrashidi *et al.*, 2021[23] to evaluate the bactericidal activity of the test samples. The selected contact time and pH values were chosen based on their relevance to the release kinetics of the encapsulated lactoferrin (ALG:Lf@CHT) (Table 1).

A concentration of 0.5 mg mL^{-1} of free and encapsulated Lf was added to 6-well plates containing 10 mL of a 0.9% NaCl bacterial suspension at an initial microbial load of 10^6 CFU per mL. The samples were maintained under constant agitation at 37 °C (SD ± 1) for the chosen contact time. Negative controls consisted of bacterial suspensions without any test substance, while positive controls were prepared by adding Ciprofloxacin at 0.5 mg mL^{-1}. Aliquots were collected immediately after adding the test substances (t_0) and at the end of the contact periods. Antibacterial efficacy was evaluated by quantifying the number of viable bacteria remaining in each treated sample.

Table 1 Summary of the experimental conditions used for antimicrobial activity investigation[a]

pH tested	Time of contact (t_1)
5	1 h 5′
7	25 h
8.5	4 h

[a] pH and the relative contact time between the substances and the bacteria.

The residual microbial load was calculated as CFU per mL at each time point, expressed as a percentage of the CFU per mL observed in the corresponding negative control. The bacterial reduction (die-off rate) was determined using the formula: 100 Residual Rate. Microbiological analyses were conducted following ISO standard specific to each microorganism: *S. aureus* was plated on a Baird Parker agar base (Thermo Fisher Scientific, USA, UNI EN ISO 6888-1:2021), *P. aeruginosa* on *Pseudomonas agar* base (Thermo Fisher Scientific, USA, UNI EN ISO 13720:2010) and *E. coli* on TBX agar (Liofilchem, Italy, UNI EN ISO 16649-1:2018).

To ensure data reliability, all experiments were carried out in three independent replicates. Sampling was performed immediately after inoculation (t_0), at 1 h 5′, at 4 h and 25 h (t_1) to assess bacterial survival and calculate microbial reduction. Results are presented as mean values ± standard deviation of the mean (SE) for each tested compound. Statistical analysis was conducted using two-way ANOVA (GraphPad Prism Software v9, GraphPad Software, La Jolla, CA, USA) to compare treated samples to the negative control at the corresponding time points. Statistical significance was set at $p < 0.05$ and is reported as $*p < 0.05$, $**p < 0.01$, $***p < 0.001$ and $****p < 0.0001$.

3. Results and discussion

3.1. Preparation of microparticles

The core–shell ALG:Lf@CHT microparticles were synthesized through a carefully controlled two-step process. Initially, alginate microparticles encapsulating lactoferrin (ALG:Lf) were produced *via* ionic cross-linking, achieved by dropwise addition of a sodium alginate solution containing Lf into a calcium chloride ($CaCl_2$) bath. The divalent Ca^{2+} ions induced rapid gelation of the alginate polymer chains, resulting in the formation of spherical microparticles with efficient protein entrapment and preserved bioactivity.[6] The conditions—including alginate concentration, Ca^{2+} concentration, and cross-linking time—were optimized to balance particle size, encapsulation efficiency, and mechanical stability.

In the subsequent step, a chitosan (CHT) coating was applied by incubating the ALG:Lf particles in a mildly acidic chitosan solution. The positively charged protonated amine groups of chitosan physically interacted with the negatively charged carboxylate groups on the alginate surface, leading to the formation of a robust core–shell structure. This coating enhanced the mechanical integrity of the microparticles, conferred pH-responsive swelling and degradation behaviors, and introduced intrinsic antimicrobial properties. Moreover, the chitosan shell served as a diffusion barrier that modulated lactoferrin release, enabling more controlled and sustained delivery, especially under variable pH conditions commonly found in infected tissues.

Overall, this two-step fabrication approach leveraged the complementary properties of alginate and chitosan to create a

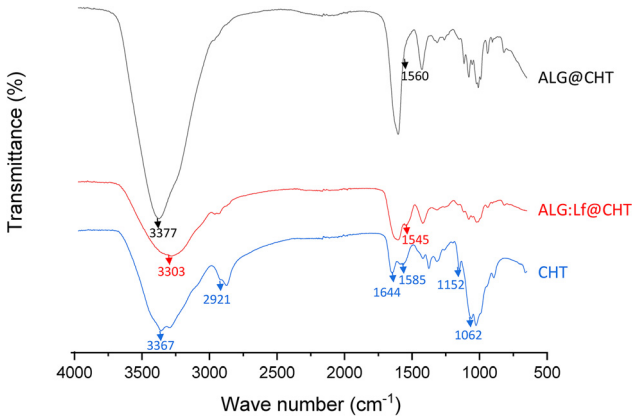

Fig. 1 FTIR-ATR spectra of ALG@CHT and ALG:Lf@CHT microparticles.

versatile delivery system with improved stability, responsiveness, and therapeutic potential.

3.2. Structural analysis

The FTIR-ATR spectra of the synthesized core–shell particles are shown in Fig. 1. The CHT peak at 3367 cm^{-1} indicated the –OH and –NH stretch overlap, while the 2921 cm^{-1} peak was due to the C–H stretch. The observed peaks at 1644, 1585, 1152, and 1062 cm^{-1} were due to the NH–CO stretch, N–H bend, and bridge –O stretch, and C–O stretching, respectively.[24]

The presence of the CHT shell was confirmed in both ALG@CHT and ALG:Lf@CHT samples by a shift in the signal of OH and –NH stretch overlap from 3367 to 3303 cm^{-1} and to 3377 cm^{-1}, respectively. This is due to the interaction of amine groups of CHT with the carboxylic groups of ALG. In addition, the shift of the N–H bend peak is also observed from 1585 cm^{-1} to 1560 and 1545 cm^{-1} for ALG@CHT and ALG:Lf@CHT, respectively.[17]

The basic peaks of both ALG and Lf components are observed also in ALG@CHT and ALG:Lf@CHT spectra.[6]

3.3. Morphological analysis

The morphological analysis of the freeze-dried ALG@CHT (Fig. 2a) and ALG:Lf@CHT (Fig. 2b) core–shell microparticles was preliminarily performed by optical microscopy observations.

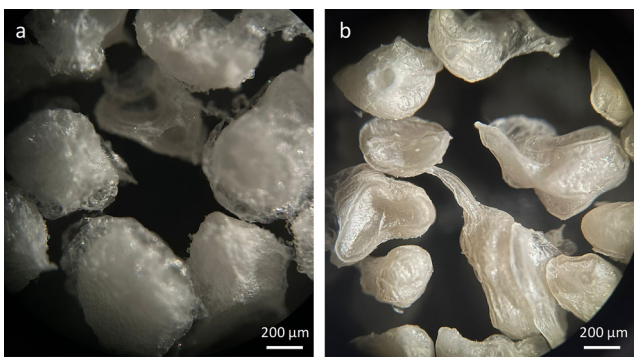

Fig. 2 Optical microscopy images of ALG@CHT and ALG:Lf@CHT microparticles.

The optical microscopy images clearly show a compact external surface of the microparticles due to the deposition of the chitosan shell on the external surface of the ALG and ALG:Lf particles.[6] In particular, the presence of Lf gives the loaded ALG:Lf@CHT core–shell a more yellow color compared to the same neat particles.

The morphological analysis of the swollen core–shell ALG@CHT (Fig. 3a) and ALG:Lf@CHT (Fig. 3b) microparticles was carried out by SEM observations. The samples were pretreated with liquid nitrogen and crushed. The SEM images of both microparticles clearly show a chitosan coating layer on the surface microparticles. This layer appears as a veil and confirms the deposition of the chitosan shell.

The freeze-dried neat ALG@CHT (Fig. 4a) particles show a round shape, while the loaded ALG:Lf@CHT (Fig. 4b) particles show an elongated shape due to the lactoferrin protein incorporated. The SEM images of both core–shell ALG@CHT and ALG:Lf@CHT particles show the chitosan coating layer, which appears as a crumpled veil deposited on the surface of the microparticles.

3.4. Thermal analysis

The thermal decomposition process of the loaded core–shell particles and their pure counterparts was evaluated by TGA.

The inflection points of the thermal decomposition curves are reported in Fig. 5 and 6, which define the degradation characteristics and simultaneously the percentage mass loss during thermal decomposition.

The freeze-dried ALG particles show a three-phase decomposition mechanism, with a percentage mass loss of 70% and a degradation temperature of ~255 °C in agreement with the results reported by Paduano *et al.*[6] (Fig. 5). Chitosan decomposed in two successive phases, with a percentage mass loss of about 70% and a higher degradation temperature (~295 °C). The core–shell ALG@CHT samples show a similar degradation mechanism to the only-ALG particles, although the chitosan shell around the particle slightly increases the degradation temperature (~260 °C). The first stage of the decomposition process of ALG and ALG@CHT particles occurs between 95 and 200 °C and is due to the mass loss through the vaporization of volatile components, such as water present in the coating (polymer dehydration). The same behavior occurs for the core–shell ALG:Lf@CHT particles loaded with Lf (Fig. 6).

In Fig. 6, it is interesting to note that the loading of the Lf protein inside the particles increases the thermal stability and degradation temperature of the loaded particles. It was observed that the core–shell samples (ALG@CHT and ALG:Lf@CHT) showed a lower mass of free water lost in the early decomposition stage. Furthermore, a higher temperature was required to release the absorbed water compared to the ALG-only sample. This behavior may be caused by a higher immobilization of water molecules between the chitosan chains. Considering the structure of chitosan and alginate, water molecules can be bound by the polar groups of alginate and chitosan: carboxyl, hydroxyl and amine.[25] Thermal degradation of the ALG carboxyl groups in the $CaCO_3$ structure

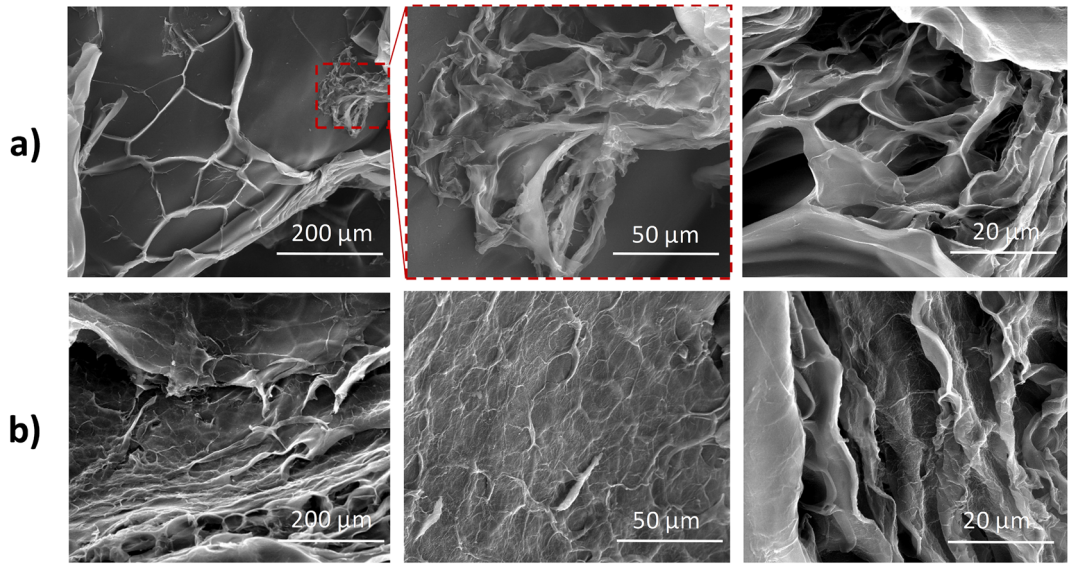

Fig. 3 SEM images of (a) ALG@CHT and (b) ALG:Lf@CHT swollen microgels, at different magnifications.

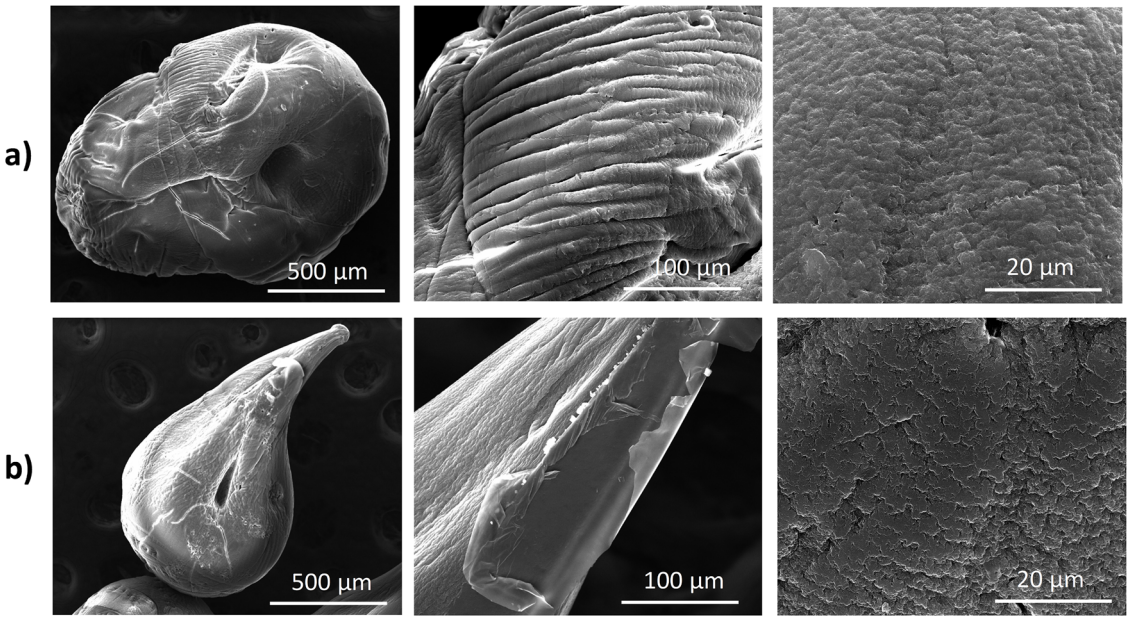

Fig. 4 SEM images of (a) ALG@CHT and (b) ALG:Lf@CHT freeze-dried microparticles.

occurs in the temperature range of 190–200 °C. In the temperature range of 250–300 °C, the percent weight loss can be attributed to the cleavage of glycosidic bonds in the alginate backbone and to the deacetylation and partial depolymerization of the chitosan chain which is observed for both CHT alone and core–shell particles. The ALG@CHT and ALG:Lf@CHT samples exhibit a third inflection point which may be due to the decomposition of the polyelectrolyte complex between the two polysaccharides, which confirms the presence of the chitosan shell. The final residue for the ALG@CHT microparticles was 12% and for the Lf-loaded core–shell particles (ALG:Lf@CHT) it was about 30% of their total weight, due to the loaded Lf. DSC analysis (Fig. S1, SI) showed similar thermal profiles for all samples with no marked shifts in glass transition or melting points upon Lf encapsulation or CHT coating.

3.5. Size measurement

The sizes of the core–shell ALG@CHT and ALG:Lf@CHT microparticles were measured using ImageJ software and were expressed as a weighted average of the diameter. Table 2 shows the particle sizes of the freshly synthesized swollen microgel

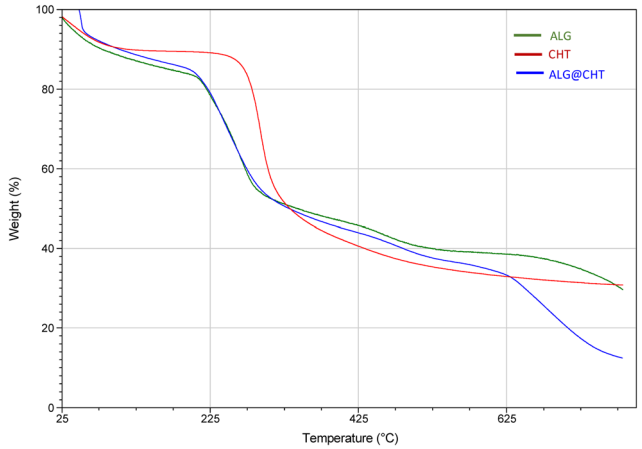

Fig. 5 Thermogravimetric curves of ALG, CHT and ALG@CHT core–shell microparticles.

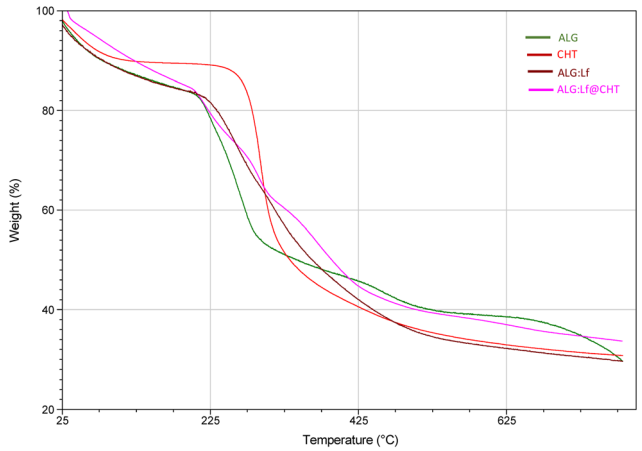

Fig. 6 Thermogravimetric curves of ALG, CHT and Lf-loaded ALG:Lf and ALG:Lf@CHT microparticles.

and of the rehydrated freeze-dried one. The rehydrated particles (r-ALG@CHT and r-ALG:Lf@CHT) recover their original shape, losing only 5–6% of their swelling power. The core–shell ALG@CHT particles are bigger than the Lf-loaded ones. This similar behavior is shown by Paduano *et al.*[6] for ALG and ALG:Lf particles.

The size distribution of the swollen core–shell ALG@CHT and ALG:Lf@CHT particles is shown in Fig. 7.

Table 2 Size measurement of microparticles[a]

Sample	Average diameter (cm)
ALG@CHT	0.24 ± 0.03
ALG:Lf@CHT	0.21 ± 0.02
r-ALG@CHT	0.18 ± 0.02
r-ALG:Lf@CHT	0.16 ± 0.01

[a] The swollen synthesized microparticles were named ALG@CHT and ALG:Lf@CHT, whereas the rehydrated ones were identified as r-ALG@CHT and r-ALG:Lf@CHT.

Fig. 7 presents the corresponding size distribution of the core–shell microspheres. The average diameter of the Lf-free core–shell microspheres is greater than those of the Lf-loaded ones. The size distribution of the core–shell particles was found to be broad and asymmetric, with sizes ranging from 0.15 to 0.35 cm as shown in Fig. 7.

3.6. Swelling index

The swelling degree (Q) of freeze-dried ALG@CHT and ALG:Lf@CHT microparticles was calculated at different times and is reported in Table 3 and the corresponding graph is given in Fig. 8. A rapid swelling of both microparticles (neat and Lf loaded) can be observed within the first hour reaching the equilibrium at longer times (in a 24–48 h range). However, for the ALG:Lf@CHT sample, the rate and degree of swelling are reduced due to the presence of a high steric hindrance molecule as lactoferrin. Compared to ALG-only and ALG:Lf microspheres,[6] Q of the core–shell microparticles were significantly reduced. This result suggested that the chitosan shell significantly tuned the swelling profiles of the microsphere.

3.7. *In vitro* release studies

In vitro release tests on Lf-loaded core–shell particles were performed on the freeze-dried samples to ensure higher stability of the encapsulated protein. The release profile of Lf was expressed as the cumulative protein concentration (%) over time in different pH environments.

The release mechanism is based on the diffusion of the active ingredient from the polymer matrix towards the external bulk.[26]

To understand the release behavior of the core–shell particles, three different pH values were chosen: 5, 7 and 8.5. These pH values were representatively for:

– normal skin, which maintains a slightly acidic pH value ($4 < pH < 6$)

– acute wound characterized by a neutral pH of ~7 due to the exposure of internal fluid and tissue

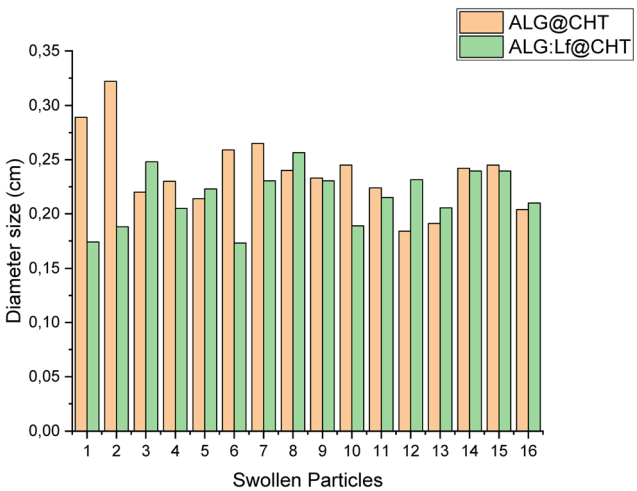

Fig. 7 Size distribution of the swollen core–shell ALG@CHT and ALG:Lf@CHT particles.

Table 3 Swelling degree Q (%) calculated from the weight of core–shell microspheres

	Q (%)				
Sample	1 h	3 h	5 h	24 h	48 h
ALG@CHT	160.3 ± 10.4	220.1 ± 8.2	380.4 ± 7.1	450.2 ± 12.6	462.3 ± 18.2
ALG:Lf@CHT	87.4 ± 5.6	95.2 ± 8.4	142.7 ± 12.2	230.6 ± 16.4	224.1 ± 6.5

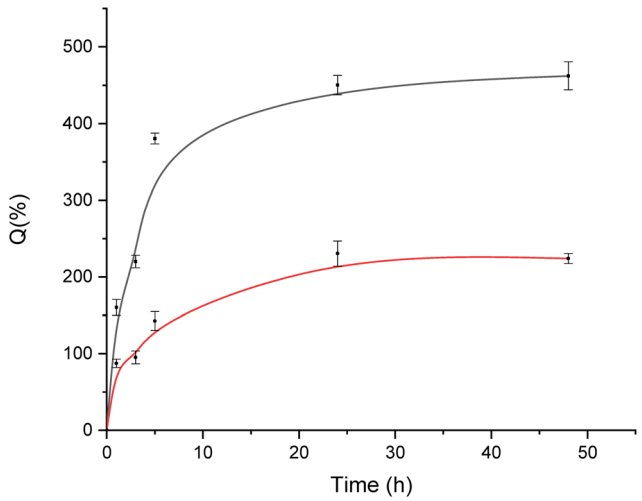

Fig. 8 Swelling degree (Q (%)) of core–shell microparticles: interval plots of ALG@CHT (black curve) and ALG:Lf@CHT (red curve) particles.

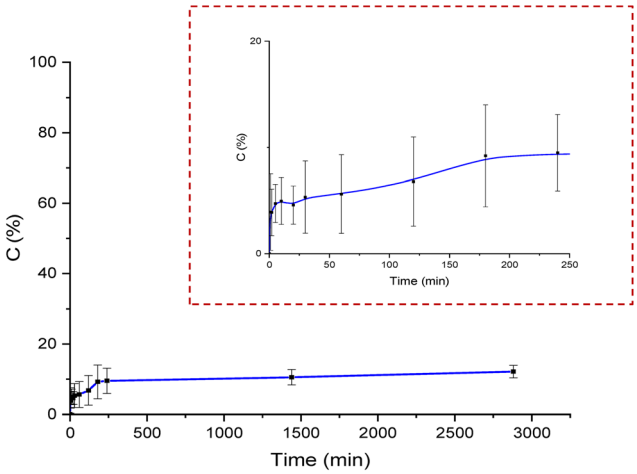

Fig. 9 *In vitro* Lf release profile from the loaded core–shell ALG:Lf@CHT particles at neutral pH.

– chronic wounds with a more alkaline pH value of 7 < pH < 9, due to factors such as interstitial fluids, blood, and ammonia.[27]

The Lf release profile at neutral pH is shown in Fig. 9. The release tests were conducted on 3 batches, and in 24 h only 10.3% (SD ± 1.52) of the trapped lactoferrin was released. Paduano *et al.*[6] revealed that the ALG:Lf microparticles released 40% of loaded Lf in 24 h. These results demonstrated that the chitosan shell around the microparticles slows down the release of the protein under neutral conditions, making the core–shell system a good solution for prolonged controlled release of active molecules. Lf has an isoelectric point 8 < PI < 8.4 and in a neutral environment it is positively charged, unlike alginate that has 3 < pK_a < 4 and is negatively charged, while the chitosan shell also has a positive charge due to the protonated amino groups.[28] This alternation of charges probably generates an attractive effect between the different components of the core–shell particles which generate a prolonged release of the encapsulated active principle over time.

At acidic pH, 88.7% (SD ± 6.4) of the encapsulated lactoferrin (Lf) was released within the first 10 minutes (Fig. 10), indicating a markedly accelerated release compared to neutral pH conditions, where only 40% of Lf was released over a 24-hour period. These findings align with the data reported by Paduano *et al.*,[6] who observed that uncoated ALG:Lf microparticles released 90% of Lf in just 6 minutes under the same mild acidic conditions. While the overall release trend is similar, the slightly slower release observed in the current study confirms the moderating effect of the chitosan coating.

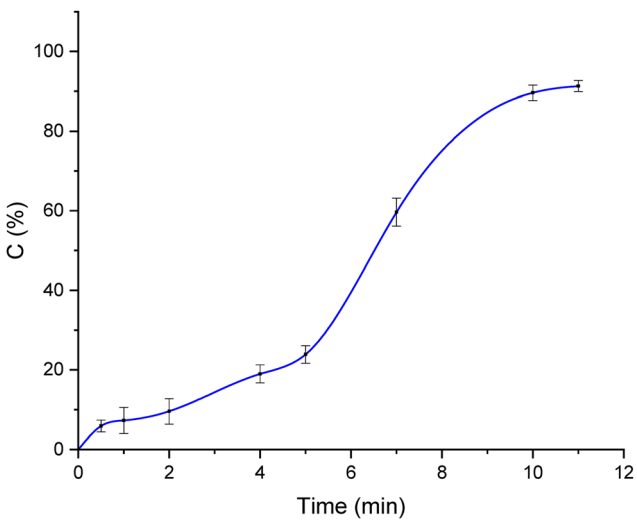

Fig. 10 *In vitro* Lf release profile from loaded core–shell ALG:Lf@CHT particles at pH 5.

The presence of the chitosan shell appears to slow down the initial diffusion of the protein, enabling a more controlled release profile compared to uncoated systems. Nevertheless, under acidic conditions, the release rate is still significantly enhanced. This behavior can be attributed to the protonation of

chitosan's amino groups at low pH, which generates electrostatic repulsion between positively charged polymer chains. This repulsion facilitates the penetration of water molecules, leading to increased chain mobility, polymer solvation, and ultimately partial dissolution of the chitosan shell.[29] As a result, while the chitosan layer effectively acts as a diffusion barrier during the initial stages of release, it progressively loses this function as the shell dissolves in the acidic environment. Consequently, the system exhibits a two-phase release behavior: an initially moderated release due to the intact chitosan coating, followed by a rapid release once the barrier effect is diminished.

In Fig. 11 the Lf release profile from the core–shell particles at pH 8.5 is shown.

At alkaline pH, the release of Lf from core–shell particles is 90.6% (SD ± 3.1) within about an hour and a half. Fig. 11 shows an initially more controlled release, which becomes faster over time.

This behavior is due to the amino groups of chitosan that are deprotonated at basic pH, losing their positive charge. In this form, the chitosan molecules are no longer soluble and precipitate, losing the barrier effect. It is observed that the turbidity of the release solution increases over time and becomes opalescent.

In a basic environment, the different components of the core–shell particles are probably negatively charged, and the repulsive forces between the molecules increase, helping the penetration of the solvent molecules into the particles and the diffusion of the Lf towards the external bulk.[30]

3.8. Encapsulation of lactoferrin (Lf)

The encapsulation efficiency EE and loading capacity LC were calculated as 55.4% (SD ± 14.1) and 26.93% (SD ± 13.6), respectively. These results suggested the possible use of the obtained Lf-loaded core–shell particles for *in vivo* applications.

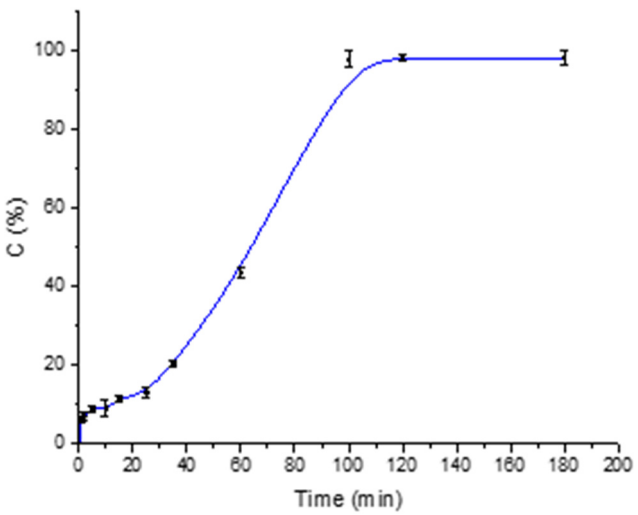

Fig. 11 *In vitro* Lf release profile from core–shell particles at pH 8.5.

3.9. Z-potential and particle size distribution of microparticles in solution

The Z-potential in a weakly acidic environment (pH 5) confirms that the incorporation of Lf into core–shell microgels improved their surface charge, as demonstrated by a higher absolute value of potential (Table 4). This suggests improved suspension stability due to increased electrostatic repulsion between particles, preventing aggregation and maintaining colloidal dispersion over time. Furthermore, the lactoferrin-loaded sample showed a significantly smaller particle size, indicating that the protein may have reduced the particle size by promoting a more compact structure, probably due to the opposite charges between the components that make up the core–shell particles. This compaction effect could improve Lf delivery efficiency, allowing better penetration into biological environments. The loaded core–shell particles show a slightly lower PDI, suggesting a more uniform distribution of particle sizes, contributing to a more homogeneous dispersion. This homogeneous dispersion is crucial for controlled release applications, as it minimizes variability and ensures predictable behavior under physiological conditions. The improved uniformity and stability of the formulation could be beneficial for preventive medical applications, ensuring consistent interaction with biological targets and reducing unwanted aggregation effects in suspension-based delivery systems.

From Z-potential analysis in a weakly alkaline environment (pH 8.5), it was found that the incorporation of Lf into the core–shell particles, resulted in an increase in particle size (Table 5). This can be attributed to the presence of the glycoprotein which likely contributed to the overall microgel size. In addition, interactions between Lf and the CHT shell may further influence the microgel size, leading to structural modifications at the molecular level. The PDI values showed that the Lf-loaded microparticles had a slightly broader size distribution than those without Lf, likely due to the heterogeneous nature of the protein encapsulation process. This suggests that the incorporation of Lf not only impacted the particle size but also introduced some variability in the particle size distribution, contributing to minor variations in microgel dimensions.

In fact the pH influences the size distribution as shown in Fig. 12, where it is clear that the alkaline condition allows a more homogenous intensity dispersion of the microparticles in solution. However, both under pH 5 and pH 8.5, the presence of the protein led to the achievement of a higher degree of uniformity (Fig. 12). In addition, Z-potential values confirmed that both microparticles exhibited a negative surface charge. As

Table 4 Z-potential, Z-size and PDI of the microparticles at pH 5[a]

Sample	Z-size (d.nm)	PDI	Z-potential (mV)
ALG@CHT	299.20 ± 15.68	0.474 ± 0.04	−12.90 ± 0.50
ALG:Lf@CHT	182.63 ± 0.38	0.379 ± 0.01	−22.10 ± 0.26

[a] The particle size distribution (Z-size), PDI (polydispersity index) and the surface charge potential (Z-potential) of the core–shell microparticles loaded with and without Lf at pH 5.

Table 5 Z-potential, Z-size and PDI of the microparticles at pH 8.5[a]

Sample	Z-size (d.nm)	PDI	Z-potential (mV)
ALG@CHT	491.97 ± 10.35	0.521 ± 0.03	−17.57 ± 0.07
ALG:Lf@CHT	721.43 ± 13.05	0.610 ± 0.05	−32.47 ± 0.22

[a] The particle size distribution (Z-size), PDI (polydispersity index) and the surface charge potential (Z-potential) of the core–shell microparticles loaded with and without Lf at pH 8.5.

demonstrated by Zhu *et al.*,[31] Lf-loaded microparticles showed a more negative Z-Potential due to the presence of both the protein and the chitosan shell, enhancing the overall negative surface charge. The increase of the Z-Potential value is critical to improving the colloidal stability of microparticles, as a greater electrostatic repulsion between particles minimizes aggregation and supports dispersion stability.

In summary, the incorporation of Lf into the alginate–chitosan core–shell microparticles induced significant modifications in their physical properties under both acidic (pH 5.0) and alkaline (pH 8.5) conditions.

These findings underscore the positive influence of Lf on microgel stability, promoting enhanced colloidal dispersion, surface charge regulation, and uniformity in particle size distribution. The observed structural adjustments highlight the potential of Lf-loaded microgels for biomedical and pharmaceutical applications, where stability and controlled release are crucial factors for therapeutic efficiency. Given their improved physicochemical characteristics, these microgels may serve as promising candidates for drug delivery systems and preventive medical interventions, offering tailored adaptability to diverse physiological environments.

3.10. Antibacterial efficacy

In this study, several tests were performed to evaluate the antibacterial activity of both free (ALG@CHT) and loaded bovine apo-Lf (ALG:Lf@CHT) core–shell particles, against different Gram-positive and Gram-negative bacterial strains: *S. aureus*, *P. aeruginosa*, and *E. coli*. The pH levels tested (5, 7, 8.5) were investigated at different incubation times. For free and encapsulated Lf, a concentration of 0.5 mg mL^{-1} was used. All samples were analyzed in triplicate in three independent tests for each growth phase.

The data on growth inhibition (%) at all pH levels tested for the different strains are summarised in Fig. 13. The tested contact time between substances and strains (10^6 CFU per mL) at pH 5 is 1 h 5 min, which was chosen according to the release kinetics at a mildly acidic environment, corresponding to a fast release of 90% of the loaded Lf within 11 min. It was observed that apo-Lf (0.5 mg mL^{-1}) had a low activity at pH 5, both in the free and loaded state (ALG:Lf@CHT) against all the evaluated pathogens. The low activity may not be due to the acidic pH, but rather the short time used in this set-up. In earlier research, it has been demonstrated that even CHT alone requires a specific incubation period before it can inhibit growth.[32] Also Erdem *et al.*,[33] evaluated the antibacterial action of CHT alone and observed that it, at acidic pH, gives good results on *S. aureus*. However, they also found that the action increases with contact time from 4 to 24 h, with a reduction in microbial load of up to 1.9 log compared to the control. Moreover, in the study, they used a concentration of 5 mg mL^{-1}, which is much higher than that used in the present study. In addition, the citrate ion can also inhibit the bacteriostatic activity of lactoferrin.[34,35] The better reduction rates ~83%, were obtained for the neat ALG@CHT core–shell system without Lf tested on *E. coli* and *P. aeruginosa*.

At pH 7, the incubation times evaluated were longer (25h) due to the slower release kinetics of ALG:Lf@CHT particles under neutral pH conditions (10% in 24 h). The results against *S. aureus* were more satisfactory, and Table 6 shows a 99% reduction rate at 25 h, for the ALG: Lf@CHT loaded core–shell

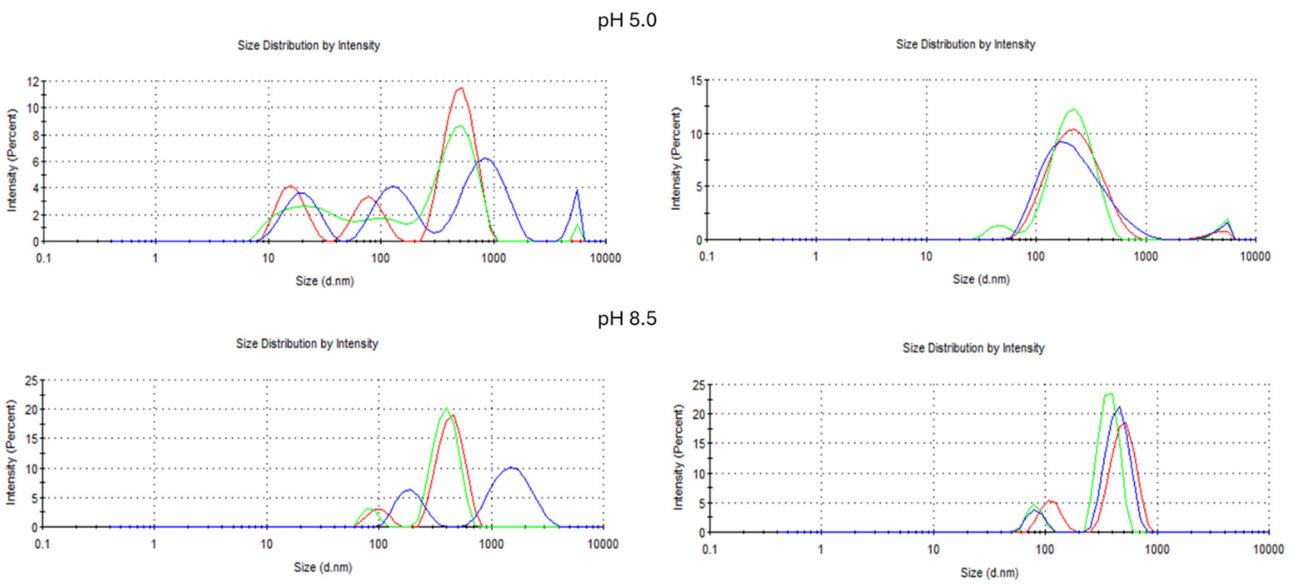

Fig. 12 Intensity particle size distribution for a mixture of ALG@CHT (left panels) and of ALG:Lf@CHT (right panels) at pH 5.0 and pH 8.5.

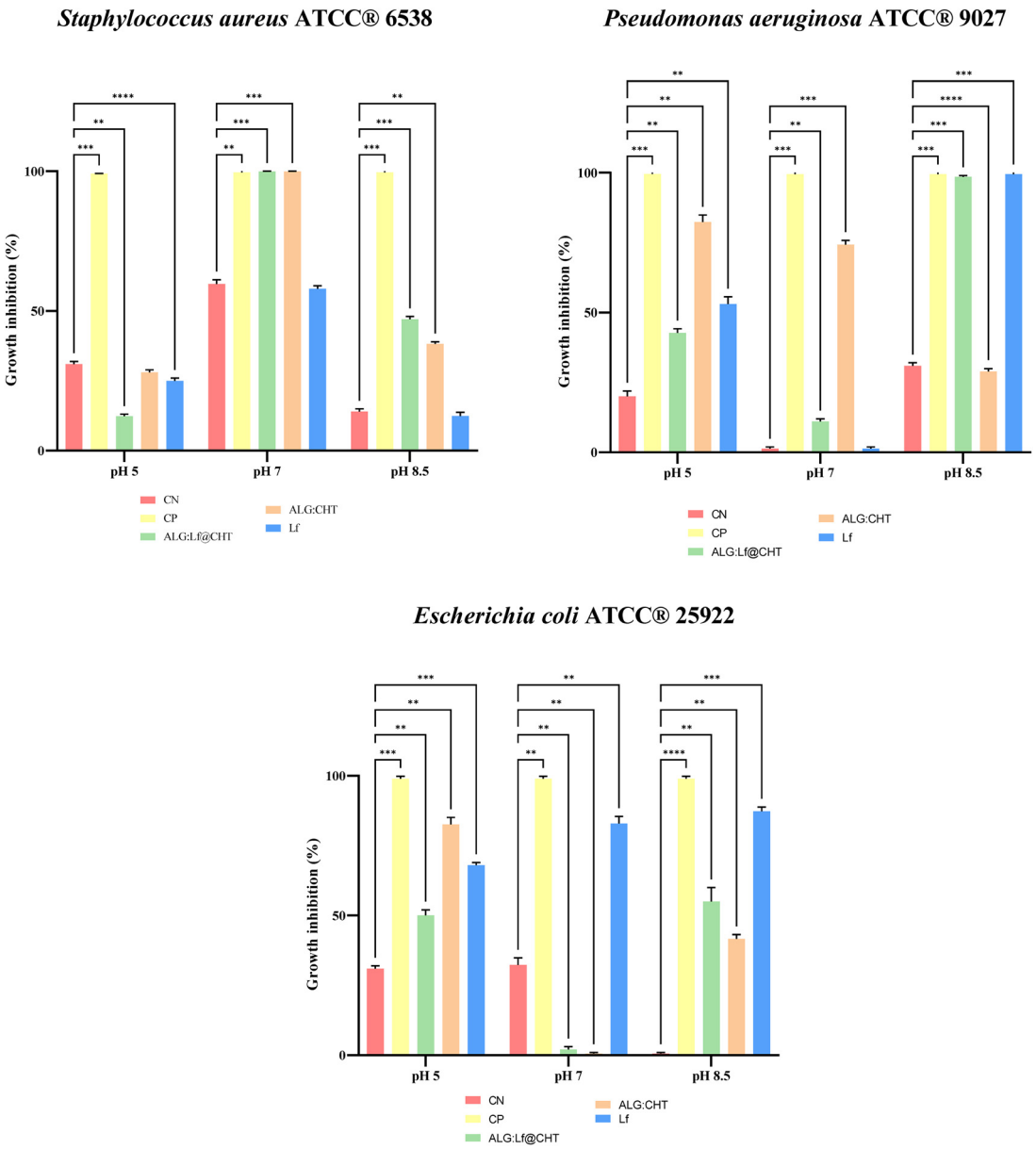

Fig. 13 Growth inhibition rate (%) of ALG:CHT, ALG:Lf@CHT and Lf, at a final concentration of 500 μg mL^{-1} against *Staphylococcus aureus* ATCC® 6538, *Pseudomonas aeruginosa* ATCC® 9027, and *Escherichia coli* ATCC® 25992. Positive control (CP) = Ciprofloxacin at 500 μg mL^{-1}; Negative Control (CN) = Inoculum of ATCC strains at 10^6 CFU per mL; values are expressed as mean (n = 3) ± standard error. Two-way ANOVA*$p < 0.05$, **$p < 0.01$, ***$p < 0.001$ and ****$p < 0.0001$.

system, and a 100% reduction rate for the neat ALG@CHT system. The results do not show an optimal activity of Lf-loaded microparticles against *E. coli* (~4%). However, a reduction rate of 76% against *P. aeruginosa* was obtained for neat ALG@CHT core–shell particles. These results suggest the possible applicability of the core–shell particles against *S. aureus* in the case of acute wounds (pH ~7). The results are given in extended form in Tables S4 and S5 in the SI.

The most satisfactory results are obtained at pH 8.5, which is the typical pH value of chronic wounds. The time evaluated was 4 h, because the kinetics of Lf release from the loaded core–shell particles (ALG:Lf@CHT) was 97% in 100 minutes. The results in Table 7 show a reduction rate of 98%, against *P. aeruginosa*, for ALG:Lf@CHT microparticles, and a 100% reduction rate for the neat ALG@CHT system, after 4 h. It is known from the literature that *P. aeruginosa*, *S. aureus*, and *E. coli* are among the pathogenic bacteria that proliferate more in the case of chronic wounds, preventing their healing. Additionally, a reduction rate of 46% against *S. aureus* and 56% against *E. coli* is obtained. These high inhibitory effects suggest the possible applicability of ALG:Lf@CHT particles against the growth of these pathogens, for epithelial healing of chronic wounds.

In summary, the various compounds tested at different pH, with lactoferrin (Lf) release times ranging from 1 to 24 hours, exhibited markedly different interactions with the target

Table 6 Microbial concentration and die-off rate [%] of *S. aureus*[a]

Viability assay at pH 7 for *S. aureus* ATCC® 6538 [10^6 CFU per mL]			
	t_0	t_1 (25 h)	
Samples	Microbial Concentration [CFU per mL]	Microbial Concentration [CFU per mL]	Die-off rate [%]
CN	$1.01 \times 10^6 \pm 9.67 \times 10^3$	$4.00 \times 10^5 \pm 1.67 \times 10^4$**	60.38
CP	$1.33 \times 10^6 \pm 8.82 \times 10^4$	$0.00 \times 10^0 \pm 0.00 \times 10^0$****	100.00
ALG:Lf@CHT	$1.18 \times 10^6 \pm 1.67 \times 10^4$	$6.67 \times 10^2 \pm 6.67 \times 10^2$****	99.94
ALG@CHT	$1.10 \times 10^6 \pm 5.77 \times 10^4$	$0.00 \times 10^0 \pm 0.00 \times 10^0$	100.00
Lf	$1.21 \times 10^6 \pm 1.35 \times 10^5$	$4.86 \times 10^5 \pm 4.46 \times 10^4$	59.66

[a] *S. aureus* ATCC® 6538 was tested at pH 7 after 25 hours with ALG:Lf@CHT and ALG@CHT at 0.5 mg mL^{-1}. Two-way ANOVA followed by Šídák's multiple comparisons test (*$p < 0.05$, **$p < 0.01$, ***$p < 0.001$, ****$p < 0.0001$).

Table 7 Microbial concentration and die-off rate [%] of *P. aeruginosa*[a]

Viability assay at pH 8.5 of *Pseudomonas aeruginosa* ATCC® 9027 [10^6 CFU per mL]			
	t_0	t_1 (4 h)	
Samples	Microbial Concentration [CFU per mL]	Microbial Concentration [CFU per mL]	Die-off rate [%]
CN	$1.20 \times 10^6 \pm 1.15 \times 10^5$	$8.03 \times 10^5 \pm 4.70 \times 10^4$	29.72
CP	$1.33 \times 10^6 \pm 1.67 \times 10^4$	$0.00 \times 10^0 \pm 0.00 \times 10^0$****	100.00
ALG:Lf@CHT	$1.07 \times 10^6 \pm 6.67 \times 10^4$	$2.13 \times 10^4 \pm 1.49 \times 10^4$	98.00
ALG@CHT	$1.46 \times 10^6 \pm 3.31 \times 10^5$	$1.03 \times 10^6 \pm 3.33 \times 10^4$	29.06
Lf	$1.41 \times 10^6 \pm 3.01 \times 10^5$	$0.00 \times 10^0 \pm 0.00 \times 10^0$*	100.00

[a] *P. aeruginosa* ATCC® 9027 was tested at pH 8.5 after 4 hours with ALG:Lf@CHT and ALG@CHT at 0.5 mg mL^{-1}. Two-way ANOVA followed by Šídák's multiple comparisons test (*$p < 0.05$, **$p < 0.01$, ***$p < 0.001$, ****$p < 0.0001$).

microorganisms. Regarding the pathogen *S. aureus*, no statistically significant effects were observed for any of the tested compounds at acidic or basic pH. However, at neutral pH, a notable antibacterial effect was detected for both the ALG@CHT and ALG:Lf@CHT formulations. In contrast, free Lf did not exhibit the same activity, suggesting that the observed antibacterial effect is likely attributable to the ALG@CHT matrix itself rather than the release of Lf from the ALG:Lf@CHT complex. In the case of *E. coli*, free Lf demonstrated the most pronounced antibacterial activity, particularly at pH 7 and 8.5. However, this efficacy was not mirrored by the synthesized compounds, which did not replicate the same behavior. Finally, against *P. aeruginosa*, ALG@CHT displayed antibacterial activity at acidic and neutral pH, although this effect diminished under basic conditions. Under these latter conditions, both free and encapsulated Lf showed increased activity, indicating efficient Lf release from the ALG:Lf@CHT system. Overall, while further optimization of the Lf release conditions is warranted, the results are promising and suggest the potential application of this system against *P. aeruginosa* in alkaline environments. In this regard, it is known that chronic and acute wounds are characterized by alkaline pH values (between 7.15 and 8.9),[36] which tend to reach neutrality and acidity during the healing process.[37] Environmental pH plays a crucial role both in the kinetics of release of the active ingredient and in the healing and treatment phases of chronic and acute wounds. Re-epithelialization and synthesis of extracellular matrix components can be enhanced by Lf, which promotes the proliferation and migration of fibroblasts and keratinocytes.[38] Therefore, topical administration of Lf contributes to the regeneration of skin wounds with a stimulatory effect due to its immunomodulatory properties.[39,40]

The results are promising, particularly given that the Lf concentrations tested are low compared to those reported in similar studies. For instance, it was recently seen that the MIC of the ALG:Lf@CHT complex towards an ETEC isolated from pigs (Enterotoxigenic *E. coli*) was 12.5 mg mL^{-1}.[41] In general, the response of pathogenic microorganisms to Lf alone is highly variable, depending very often on the individual strain and its virulence.[42] It was found that the MIC of Lf for some species of *Salmonella enterica* was even higher than 100 mg mL^{-1},[43] whereas in other studies, even values above 200 mg mL^{-1} of Lf had no effect.[44] However, in a study which evaluated the action of ALG:CHT microparticles against *S. aureus* and *P. aeruginosa*, concentrations of 20 μg were sufficient to obtain halos of inhibition of 12 and 6 mm, respectively.[45] Our study, which was carried out on the antibacterial properties of the compound against *E. coli*, *P. aeruginosa* and *S. aureus*, is preliminary and was used as an initial screening to assess the optimal conditions of use. This study provides promising preliminary evidence supporting the antibacterial potential of ALG@CHT and ALG:Lf@CHT systems, particularly under physiologically relevant pH conditions. Notably, there is increased activity against *S. aureus* at neutral pH, which supports the idea that chitosan-based matrices have intrinsic antimicrobial effects against Gram-positive bacteria. The enhanced effect at

neutral pH, which is close to the natural environment of the skin, highlights the potential for topical formulations. Furthermore, both free and encapsulated Lf demonstrated increased activity at basic pH, which mirrors the typical conditions of chronic wounds, and this was found to be the case against *P. aeruginosa*. The pH-responsive behaviour of the matrix is particularly relevant for wound healing applications, where pH modulations can optimise therapeutic outcomes. In order to further optimise the process, higher concentrations of incorporated Lf could be tested, with the tests being performed taking into account the MIC of the compound. Furthermore, depending on the end use of the product, *e.g.* in topical creams for wound treatment, synergy in enhancing the antibacterial action of incorporated Lf with other substances, such as antibiotics and probiotics, could be evaluated.

Conclusions

In this work, lactoferrin-loaded alginate particles coated with a chitosan shell (in a core–shell architecture) were prepared by a simple two-step procedure and characterized.

In vitro studies on the release kinetics of the freeze-dried system were carried out at different pH values. The results demonstrated that the deposition of a second polymeric layer on the particle can affect both the stability and the controlled release of lactoferrin at different pH values, extending the release times. In addition, the antibacterial activity of the synthesized core–shell particles was also investigated against *S. aureus*, *P. aeruginosa*, and *E. coli* under different pH conditions. The particles showed different interactions with the target microorganisms depending on pH. In particular, while neat core–shell particles showed a significant antibacterial effect at neutral pH, lactoferrin-loaded particles showed increased and improved antibacterial activity at pH 8.5. These promising results suggest the potential application of lactoferrin-loaded systems against *P. aeruginosa* under alkaline conditions, such as the possible use of them as a local reserve/storage of the proteins on damaged tissues, which could represent a solution to control wound healing.

Overall, the pH-responsive release behavior and the enhanced antimicrobial activity observed in this study support the potential clinical application of these systems, particularly in the development of advanced topical formulations for wound care. The designed particles could serve as localized depots for sustained lactoferrin release in chronic wounds or infected tissues characterized by altered pH profiles. Future studies will focus on *in vivo* validation, as well as on exploring potential synergistic effects with conventional antibiotics or probiotic agents, to further enhance the therapeutic efficacy and translational potential of the proposed delivery platform.

Conflicts of interest

There are no conflicts to declare.

Data availability

The data supporting this article have been included as part of the supplementary information (SI). Supplementary information (SI) is available. See DOI: https://doi.org/10.1039/d5ma00864f.

Acknowledgements

The authors thank Maria Rosaria Marcedula for the technical support in the use of FTIR and TGA equipment, Mario de Angioletti for the optical microscope, and Alessandra Aldi for technical support.

References

1 K. Y. Lee and S. H. Yuk, Polymeric protein delivery systems, *Prog. Polym. Sci.*, 2007, **32**, 669–697.
2 M. George and T. E. Abraham, Polyionic hydrocolloids for the intestinal delivery of protein drugs: alginate and chitosan - a review, *J. Controlled Release*, 2006, **114**, 1–14.
3 A. Muñoz-Bonilla, C. Echeverria, Á. Sonseca, M. P. Arrieta and M. Fernández-García, Bio-based polymers with antimicrobial properties towards sustainable development, *Materials*, 2019, **12**, 4.
4 S. Zuppolini, I. Cruz Maya, L. Diodato, V. Guarino, A. Borriello and L. Ambrosio, Self-associating cellulose-*graft*-poly(ε-caprolactone) to design nanoparticles for drug release, *Mater. Sci. Eng., C*, 2020, **108**, 110385.
5 S. Takka and A. Gürel, Evaluation of Chitosan/Alginate Beads Using Experimental Design: Formulation and In Vitro Characterization, *AAPS PharmSciTech*, 2010, **11**, 460–466.
6 T. Paduano, S. Zuppolini, R. Vitiello, M. Zarrelli and A. Borriello, Encapsulation of Lactoferrin in Calcium-Alginate Microparticles and Its Release Therefrom Under Neutral and Mild Acidic Conditions: Synthesis, Characterization and Mathematical Modeling, *Gels*, 2025, **11**, 116.
7 S. Takka and F. Acartürk, Calcium alginate microparticles for oral administration: I: effect of sodium alginate type on drug release and drug entrapment efficiency, *J. Microencapsulation*, 1999, **16**, 275–290.
8 S. Şenel and A. A. Hıncal, Drug permeation enhancement via buccal route: possibilities and limitations, *J. Controlled Release*, 2001, **72**, 133–144.
9 G. Coppi, V. Iannuccelli, E. Leo, M. T. Bernabei and R. Cameroni, Chitosan–alginate microparticles as a protein carrier, *Drug Dev. Ind. Pharm.*, 2001, **27**, 393–400.
10 L. Zhang, J. Guo, X. Peng and Y. Jin, Preparation and release behavior of carboxymethylated chitosan/alginate microspheres encapsulating bovine serum albumin, *J. Appl. Polym. Sci.*, 2004, **92**, 878–882.
11 L. G. Confederat, C. G. Tuchilus, M. Dragan, M. Sha'at and O. M. Dragostin, Preparation and Antimicrobial Activity of Chitosan and Its Derivatives: A Concise Review, *Molecules*, 2021, **26**, 3694.

12 I. Cruz Maya, S. Zuppolini, M. Zarrelli, E. Mazzotta, A. Borriello, C. Malitesta and V. Guarino, Polydopamine-Coated Alginate Microgels: Process Optimization and In Vitro Validation, *J. Funct. Biomater.*, 2023, **14**, 2.
13 N. Orsi, The antimicrobial activity of lactoferrin: Current status and perspectives, *Biometals*, 2004, 189–196.
14 J. M. Steijns and A. C. M. Van Hooijdonk, Occurrence, structure, biochemical properties and technological characteristics of lactoferrin, *Br. J. Nutr.*, 2000, **84**, 11–17.
15 R. Brighenti and M. P. Cosma, Swelling mechanism in smart polymers responsive to mechano-chemical stimuli, *J. Mech. Phys. Solid*, 2020, **143**, 104011.
16 M. Avitabile, S. F. Mirpoor, S. Esposito, G. Merola, L. Mariniello, G. T. Patanè, D. Barreca and C. V. L. Giosafatto, Manufacture of Bioplastics Prepared from Chitosan Functionalized with Callistemon citrinus Extract, *Polymer*, 2024, **16**(19), 2693.
17 P. Mukhopadhyaya, S. Maityc, S. Mandal, A. S. Chakrabortic, A. K. Prajapatia and P. P. Kundu, Preparation, characterization and in vivo evaluation of pH sensitive, safequercetin-succinylated chitosan-alginate core-shell-corona nanoparticle for diabetes treatment, *Carbohydr. Polym.*, 2018, **182**, 42–51.
18 A. Bhattacharyya, F. Nasim, R. Mishra, R. P. Bharti and P. P. Kundu, Polyurethane-incorporated chitosan/alginate core–shell nano-particles for controlled oral insulin delivery, *J. Appl. Polym. Sci.*, 2018, **135**, 46365.
19 International Organization for Standardization. (2021). ISO 6888-1:2021. Microbiology of the food chain – Horizontal method for the enumeration of coagulase-positive staphylococci (Staphylococcus aureus and other species) – Part 1: Method using Baird-Parker agar medium. Available to: https://www.iso.org/standard/76672.html [Accessed on May 3, 2025].
20 International Organization for Standardization. (2010). ISO 13720:2010. Meat and meat products Enumeration of presumptive Pseudomonas spp. Available to: https://www.iso.org/standard/45099.html [Accessed on May 3, 2025].
21 International Organization for Standardization. (2018). ISO 16649-1:2018. Microbiology of the food chain—Horizontal method for the enumeration of beta-glucuronidase-positive Escherichia coli. Part 1: Colony-count technique at 44 degrees C using membranes and 5-bromo-4-chloro-3-indolyl beta-D-glucuronide. Available to: https://www.iso.org/standard/64951.html [Accessed on May 3, 2025].
22 European Standards. (2020). UNI EN 1276:2020. Chemical disinfectants and antiseptics - Quantitative suspension test for the evaluation of bactericidal activity of chemical disinfectants and antiseptics used in food, industrial, domestic and institutional areas - Test method and requirements (phase 2, step 1) Available to: https://www.en-standard.eu/ [Accessed on May 3, 2025].
23 A. Alrashidi, M. Jafar, N. Higgins, C. Mulligan, C. Varricchio, R. Moseley, V. Celiksoy, D. M. J. Houston and C. M. Heard, A Time-Kill Assay Study on the Synergistic Bactericidal Activity of Pomegranate Rind Extract and Zn (II) against Methicillin-Resistant Staphylococcus aureus (MRSA), Staphylococcus epidermidis, Escherichia coli, and Pseudomonas aeruginosa, *Biomolecules*, 2021, **11**(12), 1889.
24 P. Mukhopadhyay, S. Chakraborty, S. Bhattacharya, R. Mishra and P. P. Kundu, pH-sensitive chitosan/alginate core-shell nanoparticles for efficient and safe oral insulin delivery, *Int. J. Biol. Macromol.*, 2015, **72**, 640–648.
25 D. Kulig, A. Zimoch-Korzycka, A. Jarmoluk and K. Marycz, Study on Alginate–Chitosan Complex Formed with Different Polymers Ratio, *Polym. J.*, 2016, **8**, 167.
26 S. R. Derkach, N. G. Voronko, N. I. Sokolan, D. S. Kolotova and Y. A. Kuchina, Interactions between gelatin and sodium alginate: UV and FTIR studies, *J. Dispers. Sci. Technol.*, 2020, **41**, 690–698.
27 I. J. Das, B. Trishna and I. Jogamaya, pH factors in chronic wound and pH-responsive polysaccharide-based hydrogel dressings, *Int. J. Biol. Macromol.*, 2024, **279**, 135118.
28 W. F. Huang, C. P. Tsui, C. Y. Tang, M. Yang and L. Gu, Surface charge switchable and pH-responsive chitosan/polymer core-shell composite nanoparticles for drug delivery application, *Composites, Part B*, 2017, **121**, 83–91.
29 H. Du, M. Liu, X. Yang and G. Z. Drug, The design of pH-sensitive chitosan-based formulations for gastrointestinal delivery, *Drug Discovery Today*, 2015, **20**, 1004–1011.
30 I. A. Sogias, V. V. Khutoryanskiy and A. C. Williams, Exploring the Factors Affecting the Solubility of Chitosan in Water, *Macromol. Chem. Phys.*, 2010, **211**, 426–433.
31 M. Zhu, L. Dongdong, L. Qing, S. Wu, W. Wang, L. A. Lyon, W. Wang, P. Bártolo, M. Dickinson and B. R. Saunders, Highly swelling pH-responsive microgels for dual mode near infrared fluorescence reporting and imaging, *Nanoscale Adv.*, 2020, **2**, 4261–4271.
32 B. Li, X. Wang, R. X. Chen, W. G. Huangfu and G. L. Xie, Antibacterial activity of chitosan solution against Xanthomonas pathogenic bacteria isolated from Euphorbia pulcherrima, *Carbohydr. Poly.*, 2008, **72**, 287–292.
33 B. Erdem, E. Kariptaş, T. Kaya, Ş. Tulumoğlu and Ö. Görgülü, Factors ınfluencing antibacterial activity of chitosan against Aeromonas hydrophila and Staphylococcus aureus, *Int. Cur. Pharm. J.*, 2016, **5**(5), 45–48.
34 F. Berlutti, F. Pantanella, T. Natalizi, A. Frioni, R. Paesano, A. Polimeni and P. Valenti, Antiviral Properties of Lactoferrin—A Natural Immunity Molecule, *Molecules*, 2011, **16**, 6992–7018.
35 N. D. Embleton, J. E. Berrington, W. McGuire, C. J. Stewart and S. P. Cummings, Lactoferrin: Antimicrobial activity and therapeutic potential, *Semin. Fetal. Neonatal. Med.*, 2013, **18**, 143–149.
36 M. Romanelli; E. Schipani; A. Piaggesi and P. Barachini, *Evaluation of surface pH on venous leg ulcers under Allevyn Dressings*, Royal Society of Medicine Press, London, 1998.
37 G. Gethin, The significance of surface pH in chronic wounds, *Wounds*, 2007, **3**, 6–52.
38 Y. Takayama, Effects of Lactoferrin on Skin Wound Healing, in *Lactoferrin and Its Role in Wound Healing*. Springer, Dordrecht, 2012.

39 S. L. Percival, S. McCarty, J. A. Hunt and E. J. Woods, The effects of pH on wound healing, biofilms and antimicrobial efficacy, *Wound Rep. Reg.*, 2014, **22**, 174–186.
40 S. Percival and C. Cochrane, Wounds, enzymes, and proteases, in *Microbiology of Wounds*, ed. Percival S. L., Cutting K., 2010, pp. 249–270.
41 A. Cots, N. M. Camacho, S. D. Palma, F. Alustiza, L. Pedraza, F. Bonino, J. Carreño, C. Flores Bracamonte, D. Acevedo, A. Bozzo and R. Bellingeri, Chitosan-alginate microcapsules: A strategy for improving stability and antibacterial potential of bovine Lactoferrin, *Int J Biol Macromol*, 2025, **307**(Pt 2), 141870.
42 F. Shahidi, S. Roshanak, A. Javadmanesh, F. T. Yazdi, Z. Pirkhezranian and M. Azghandi, Evaluation of antimicrobial properties of bovine lactoferrin against foodborne pathogenic microorganisms in planktonic and biofilm forms (in vitro), *J. Consum. Prot. Food Saf.*, 2020, **15**, 277–283.
43 E. N. Biernbaum, A. Gnezda, S. Akbar, R. Franklin, P. A. Venturelli and J. L. McKillip, Lactoferrin as an antimicrobial against Salmonella enterica and Escherichia coli O157:H7 in raw milk, *JDS Commun.*, 2021, **2**(3), 92–97.
44 F. B. de Andrade, J. C. de Oliveira, M. T. Yoshie, B. M. Guimarães, R. B. Gonçalves and W. D. Schwarcz, Antimicrobial activity and synergism of lactoferrin and lysozyme against cariogenic microorganisms, *Braz. Dent. J.*, 2014, **25**(2), 165–169.
45 R. Thaya, B. Vaseeharan, J. Sivakamavalli, A. Iswarya, M. Govindarajan, N. S. Alharbi, S. Kadaikunnan, M. N. Al-Anbr, J. M. Khaled and G. Benelli, Synthesis of chitosan-alginate microspheres with high antimicrobial and antibiofilm activity against multi-drug resistant microbial pathogens, *Microb. Pathog.*, 2018, **114**, 17–24.